Proceedings of ASME Turbo Expo 2022
Turbomachinery Technical Conference and Exposition
GT2022
June 13-17, 2022, Rotterdam, The Netherlands

GT2022-82139

Attendee Read-Only Copy

# NUMERICAL STUDY OF COMBUSTOR-TURBINE INTERACTION BY USING HYBRID RANS-LES APPROACH

**S.G.Tomasello, A.Andreini**
Department of Industrial Engineering
University of Florence
Florence, Italy
stellagrazia.tomasello@unifi.it

**R.Meloni,S.Cubeda,L.Andrei,V.Michelassi**
Baker Hughes
Florence, Italy
roberto.meloni@bakerhughes.com

## ABSTRACT

*The complex flow field of gas turbine lean combustors is meant to reduce $NO_x$ emissions and maintain a stable flame by controlling the local temperature and promoting high turbulent mixing. Still, this may produce large flow and temperature unsteady distortions capable of disrupting the aerodynamics and heat transfer of the first high-pressure-turbine cooled nozzle. Therefore, the interaction between the combustion chamber and the turbine nozzle is analyzed first with the help of scale-resolving simulations that notably also include a realistic turbine nozzle cooling system. To determine the nature and severity of the interaction, and the risks associated to performing decoupled simulation, the results of the coupled computer simulation are analyzed and compared with those of decoupled simulations. In this case, the combustor is computed by replacing the turbine nozzle with a discharge convergent with the same throat area, and the conditions at the interface plane are used as inlet boundary conditions for a conventional RANS of the nozzle. The analyses of the coupled and decoupled simulation reveal that the combustion chamber is weakly affected by the presence of the nozzle, whereas the two thermal fields of the nozzle surface differ considerably, as well as the disruption of the film cooling by the incoming flow distortions.*

Keywords: Gas turbine, Combustor, Turbine, Interaction, CFD, RANS, SBES.

## NOMENCLATURE

**Acronyms**

| | |
|---|---|
| C2+ | Hydrocarbons with two or more carbon atoms |
| CDC | Compressor Discharge Chamber |
| CFL | Courant-Friedrichs-Lewy |
| FGM | Flamelet Generated Manifols |
| DES | Detached Eddy Simulation |
| FETT | First Engine To Test |
| FTT | Flow Through Time |
| GTs | Gas Turbines |
| HPT | High Pressure Turbine |
| LE | Leading edge |
| LES | Large Eddy Simulation |
| NGV | Nozzle Guide Vane |
| PDF | Probability Density Function |
| PS | Pressure Side |
| RANS | Reynolds-Averaged Navier Stokes |
| SAS | Scale Adaptive Simulation |
| SBES | Stress-Blended Eddy Simulation |
| SGS | Sub-Grid Scale |
| SS | Suction Side |
| SST | Shear Stress Transport |
| S1N | First Stage Nozzle |
| TNH | Normalized High Pressure Turbine speed |
| TNL | Normalized Low Pressure turbine speed |

**Greek**

| | |
|---|---|
| $\Delta$ | Local cell volume |
| $\varepsilon$ | Turbulence dissipation rate |
| $k$ | Turbulent Kinetic Energy |
| $\mu$ | Dynamic viscosity |
| $\omega$ | Specific rate of dissipation |
| $\rho$ | Density |

**Symbols**

| | |
|---|---|
| $C_\mu$ | Model coefficient for the turbulent viscosity |
| $l_t$ | Turbulent lenght scale |
| S | Local strain rate magnitude |
| x,y,z | Spatial coordinates |
| $y^+$ | Dimensionless wall distance |
| u | Velocity component |


Copyright © 2022 by ASME and Baker Hughes

## INTRODUCTION

Lean burn technology is certainly the most promising and common solution for modern gas turbines (GTs) to meet the ever-increasing requirements toward $NO_x$ emissions abatement. This is accomplished by controlling the flame temperature promoting high turbulence levels and highly complex flow fields characterized by strong mixing, necessary to allow the lean flames to anchor. Such severe conditions result in highly-swirled and temperature-distorted flow field, due to the presence of large scale vorticity generated by the burner, that survives down the High Pressure Turbine (HPT), as proven both numerically and experimentally by Cha et al. [1,2]. As a consequence, the presence of such intermittent non-uniformities in velocity and temperature can alter dramatically the heat transfer and the aerodynamics of the end-walls [3,4] and of the vanes [5,6] as well, by increasing local convection heat transfer coefficients [7], potentially causing the damage of the components or affecting their efficiency. Moreover, it has been also widely demonstrated that the different swirler-to-nozzle relative clocking position influences the migration of the high swirled hot streak through the nozzle guide vane (NGV), remaining still recognizable at its exit [8–10]. This has also an effect on the behavior of the cooling system: in fact, it has been proven, both experimentally [11,12] and numerically [13,14], that such unsteady strongly non-uniform distortions can significantly alter the incidence over the height of the vane [15], leading to a deterioration of the adhesion of the film coolant and causing an increase in temperature load of the NGV surface.

The impact of large-scale flow structures on thermal boundary layers has also been demonstrated by Wissink et al. [16] who performed Direct Numerical Simulations (DNS) of a flow with intermittent separation. The simulations revealed a strong coupling between the core flow and the thermal boundary layer, as well as the inadequacy of linear turbulence model closures for both momentum and temperature mixing.

For this reason, a better understanding of the physical processes related to the combustor-turbine interaction becomes mandatory for the aerothermal design.

Even if, from a historical point of view, the combustor and the turbine have been studied separately by exchanging information through a shared interface between the two components, such decoupled approach is known to provoke potential inaccuracies. This practice does allow to reduce the computational effort by assuming a weak, and steady, interaction between the two components thereby ignoring the coupling effects on both the NGV and the flow and thermal field in the combustion chamber [17–19].

For these reasons, simulating all-together the combustion chamber and the first stage turbine nozzle at least, is preferable even if it is very challenging in terms of discretization in both time and space, due to the very different nature of the flow fields that characterize the two components.

Despite Reynolds Averaged Navier-Stokes (RANS) methodology is widely applied in the industry thanks to the low computational effort required, it has been widely demonstrated that it is unable to reproduce accurately the temperature and flow fields at the exit of the combustor due to the strong underprediction of the turbulent mixing [20,21] as also discussed by Wissink et al. [16] who analyzed the turbulence model closure with the help of DNS data base.

A valid alternative is represented by Large-Eddy Simulation (LES), which resolves the majority of the turbulent flow structures and models fine scale dissipative structures [22]. However, although its application for the study of the combustor-turbine interaction has been recently documented [23–25] and it has been applied also for industrial purpose [26], it is usually employed for simplified laboratory geometries due to the high computational effort required. Moreover, film cooling holes are generally neglected. For this reason, hybrid RANS-LES approaches have been introduced, such as Scale Adaptive Simulation (SAS) [27,28] or Detached Eddy Simulation (DES) [29] that allow to bridge the cumbersome resolution of boundary layer with URANS. Doing so, it is possible to guarantee a satisfactory accuracy with a manageable computational cost. In this regard, a critical comparison with the experiments carried out by Bacci et al. [30,31] has been made by Andreini et al. [32] by performing numerical analyses with RANS and SAS as well on a non-reactive test rig representative of a effusion cooled, lean-burn, annular combustor, developed in the context of the EU Project FACTOR (Full Aerothermal Combustor-Turbine interactiOns Research). The authors pointed out that SAS predicts better than RANS the recirculating region inside the combustor, which has a large impact over the resulting gas temperature at the turbine inlet and over the coolant and the main stream mixing process, even if it mildly affects the velocity field. As a matter of fact, even if RANS is sufficient to predict the aerodynamics of the turbine and to provide a reasonably accurate solution with a low computational effort [33], Scale-Resolving methods are required to assess satisfactorily the thermal behavior of the vanes, as demonstrated by subsequent works [34,35].

More recently, the Stress-Blended Eddy Simulation (SBES) model has been used to assess the effectiveness of a combustor-turbine integrated simulation versus modeling them separately [36]. Such innovative hybrid approach proposed by Menter [37] represents a further development of hybrid models, like SAS and DES, and it allows to avoid the computationally expensive LES in boundary layers that are modelled by RANS. In particular, the authors [36] studied first the two components by modeling them separately by a SBES of the combustor and RANS for the NGV by exchanging information between them at the interface. Then they proceeded with an integrated combustor-NGV calculation SBES. The authors pointed out that, even if studying the two components separately or all-together yielded similar accuracy by using SBES, the decoupled approach is still less efficient since it requires at least two iterative loops to converge the co-simulation model.

However, in order to assure a better understanding of the physical processes related to the combustor-turbine interaction, to the author's knowledge, much is yet to be studied on the impact of this interaction on the aerodynamics and thermal fields including film cooling holes on both the airfoil and platforms with realistic inlet condition representative of real operation.


Copyright © 2022 by ASME and Baker Hughes

Under such premises, the present work concentrates on the analysis and comparison between the numerical simulation of a fully integrated combustor-NGV configuration and a companion isolated NGV simulation, with the goal to investigate the interaction between the film cooling jets and the main hot flow coming from the combustor with a realistic annular geometry and operating conditions.

The integrated combustor-NGV case has been investigated by using a SBES, since it is able to resolve most of the flow structures while reducing the computational cost. The NGV stand-alone case has been instead investigated by performing a RANS simulation, as per standard industrial practice.

## NUMERICAL SETTING

### Combustion and turbulence models

In this paper, in order to represent the flame blush, the FGM combustion model with an extended turbulent flame speed closure for the progress variable source term is used. The mathematical implementation of this customized model can be found in Nassini et al. [38,39] and Romano et al. [40]. The approach implements the heat loss on the flame propagation and the combined effect of the strain rate, resulting in a improvement of the prediction of the flame front position and morphology with benefits in terms of accuracy for both emissions [41,42] and combustion dynamic [43]. The GRI-MECH3.0 [44] has been used to perform the pre-tabulation of the chemistry set for the flamelets generation, finally integrated into a PDF to properly consider the turbulence-chemistry interaction. Since the combustor represents only the hot gas generator for the First Stage Nozzle (S1N), no further details are provided in this paper.

The Combustor-S1N integrated case adopts the SBES approach in which under-resolved regions are bridged with the $k-\omega\,SST$ model. The resolved flow regions adopt the Dynamic-Smagorinsky SGS closure. This choice allows the computational cost to be limited while ensuring a high accuracy of the solution in the boundary layer of the S1N where the computational grid has14 prismatic layers. Here, the height of the first grid layer ensures that the $y^+$ doesn't exceed 1 all over the blade surface and in the proximity of the cooling holes.

The computations adopt a fully compressible approach due to the high Mach number in the throat section of the NGV. Such condition has a direct impact on the time step size of the SBES whose value is determined to ensure a convective CFL number of around 1.

The S1N stand-alone case is investigated only by RANS simulations with the $k-\omega\,SST$ turbulence model. The criteria used to build the computational grid are the same of the complete configuration.

## COMPUTATIONAL DOMAINS, MESH RESOLUTIONS AND NUMERICAL SETTINGS

Combustor-NGV case

Figure 1 shows the computational domain of the case with the S1N integrated with the combustor. The domain includes a plenum upstream of the swirler mimicking the CDC and allowing the velocity fluctuations at the entrance of the premixer to be accounted for. The premixer has a double counter-rotating swirler to enhance the mixing of the fuel injected through the premixed fuel line as well as the piloted fuel line [45]. The latter is responsible for the flame stabilization injecting the fuel in the primary zone of the combustor through co-axial holes [46].

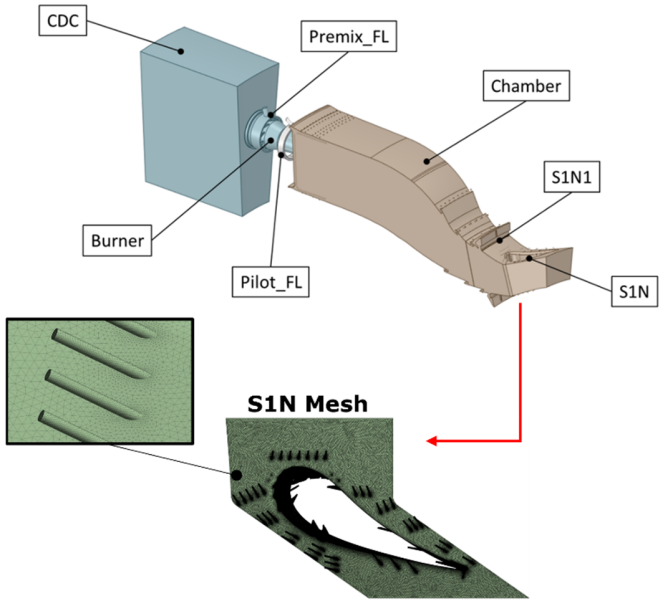


***Figure 1.*** *Computational domain of the complete model and detail view of the S1N mesh. For obvious reasons, the analysis iis limited to one-cup of the annular combustion system.* ***(© 2022 Baker Hughes Company – All rights reserved)***

The interface region between the combustor and the S1N considers also the leakage passing through the leaf seals. The employed stator geometry was specifically redesigned to have the same burners and nozzles count in order to provide a 1:1 ratio. The corresponding mass flow rates at both the inner and the outer walls upstream of the nozzle are estimated through a dedicated flow network representative of a realistic engine. The presence of these endwall flows is mandatory since they are among the main sources of the temperature distortion along the stator in both the spanwise and streamwise directions. Moreover, the long residence time of this industrial combustion chamber leads to a very homogeneous circumferential temperature distribution at plane-39.5 location (i.e. at the NGV inlet). Therefore, the impact of different swirler-to-S1N clocking positions on the performance of the nozzle guide vane is small and it does not need to be investigated for this set-up.


Copyright © 2022 by ASME and Baker Hughes

As previously mentioned, a flow network is used to predict the injection mass flow rates applied as inlet boundary conditions for the film cooling rows of the vane. Film cooling holes are modelled extending the computational domain inside the cooling channel to avoid the inaccurate prediction of cooling flow due to boundary conditions applied directly on the airfoil surface as patches. With the goal to investigate the interaction between the film cooling jets and the main hot flow coming from the combustor, the pressure-inlet boundary condition type should be more appropriate for the inlets of the S1N than the mass flow rate adopted in the present study. However, since the geometry of the cooling jets has been here simplified to limit the global cell count and the data about the total pressure to be applied refer to different locations not implemented numerically, it has been decided to preserve the total cooling flow rate. Regarding the NGV outlet boundary condition, a standard pressure outlet with a radial profile for the static pressure is implemented for both the complete case and the S1N stand-alone domain.

The mesh size of the integrated model is 84 million polyhedral elements, built from a tetrahedral grid of 365 million elements. The cell count of the S1N volume is around 20 million polyhedral elements. The mesh resolution is designed to resolve at least the 80% of the turbulent kinetic energy in the LES-modelled regions. Additionally, the limited time step-size, with an order of magnitude of $10^{-6}\ s$, makes the present analysis quite challenging from the computational cost standpoint.

Both spatial and the implicit temporal discretization schemes are at the second order accurate along with the coupled scheme for the pressure-velocity coupling. The employed solver is the commercial 3D Navier-Stokes solver ANSYS-Fluent.

S1N stand-alone case

For the S1N stand-alone case, the numerical domain has been extracted from the one including both combustor and S1N, as showed in Figure 1. The numerical simulations are carried out by using the commercial 3D Navier-Stokes solver ANSYS-CFX. As mentioned already, turbulence effects have been modelled by using the $k-\omega\ SST$ model, combined with automatic wall treatment, which applies a smooth transition between a standard wall function and a low Reynolds formulation based on the local $y^+$ value. The advection fluxes of continuity, momentum and total energy, along with the convective terms of turbulence equations, have been calculated by using a bounded high-resolution scheme, resulting in a second order accuracy. The viscous work term is included in the energy equation. The boundary condition at the stator inlet prescribes a total pressure and static temperature maps extracted from the precursor LES of the stand-alone combustor. The cooling mass flow rates and total temperature are imposed as inlet boundary conditions at the different film cooling holes, consistently to the integrated combustor-NGV case. Concerning the outlet condition of the stator, a standard radial static pressure profile has been applied, as previously mentioned. On the walls a no-slip, adiabatic, smooth wall is used.

The computational grid is generated in ANSYS Meshing consistently to the combustor-stator integrated case: the mesh size counts about 32 million of tetrahedral elements and 14 prismatic layers are adopted in the boundary layer to maintain the $y^+$ value below 1 all over the vane surfaces and cooling holes.

## OPERATING CONDITIONS

The operating conditions taken as reference for the investigation refer to the engine marching at full speed and full load during the FETT campaign. The combustor is operated with a pilot/premix ratio such that the NO15 emission was maintained below 15 ppmvd with a fuel composition having a moderate C2+ and inert content. The firing temperature of this test point was the design one. Table 1 summarizes the main information characterizing the selected operating conditions.

| **Test Point Conditions** | | |
|---|---|---|
| **Fuel Composition [% vol.]** | **CH4** | 87 |
| | **C2+** | 7.5 |
| | **Inert** | 5.5 |
| **Pilot/Premix fuel ratio [-]** | 0.36 | |
| **Ambient Temperature [°C]** | 6 | |
| **TNH, TNL [%]** | 100 | |
| **Firing Temperature** | Design value | |

**Table 1**. Operating conditions of the engine. ***(© 2022 Baker Hughes Company – All rights reserved)***

## RESULTS

Analysis of the plane 39.5 conditions and turbulent flow characteristics along the vane

The boundary conditions of the NGV stand-alone case are defined leveraging an available Large-Eddy Simulation [42] of the combustion chamber for the same engine test point. The simulation was run without the NGV at the exit, that was replaced with a convergent axisymmetric nozzle that provides a realistic back-pressure as it has the same throat area and hence Mach number of the NGV. From the time averaged solution, the 2D maps of temperature, velocity components, turbulence kinetic energy and turbulent length scale are extracted at the p39.5 location, which represents the interface between the two components, and eventually imposed as inlet boundary conditions on the same plane of the NGV RANS-based calculation.

Figure 2 compares both the 2D map and tangential averaged profiles of temperature and axial velocity at the NGV inlet section extracted from the coupled combustion chamber plus nozzle SBES (bottom) with those extracted from the precursor LES mentioned above (top). The comparison focuses on these two quantities that illustrate the most relevant features. While both the contour plot and the circumferentially-average profile

 Copyright © 2022 by ASME and Baker Hughes

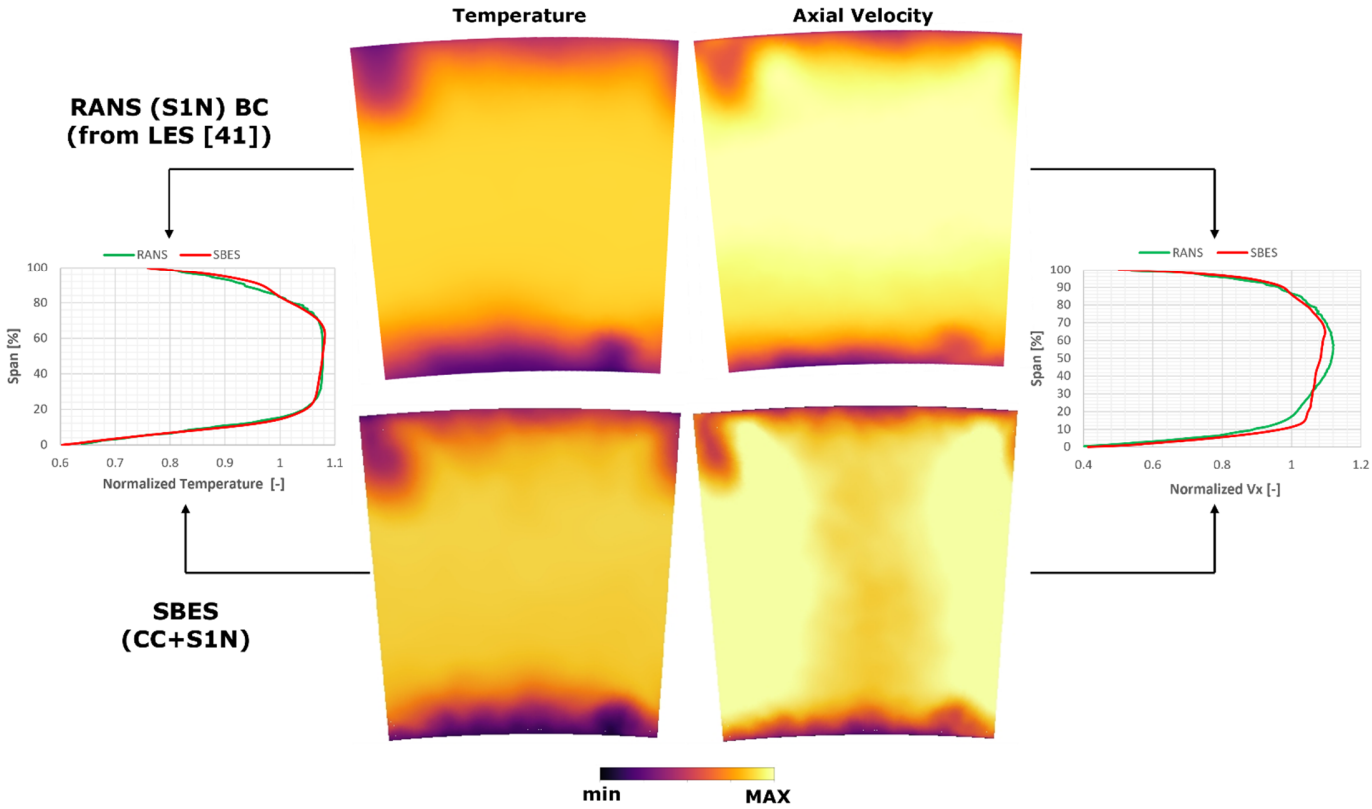


***Figure 2**. Imposed temperature and axial velocity maps for the RANS (Top) and corresponding time-averaged solution from the SBES case (bottom) at p39.5 location. While no major difference can be identified in terms of temperature, the blockage effect of the NGV alters the axial velocity profile. Both profiles have been normalized using the mass-weighted values.* ***(© 2022 Baker Hughes Company – All rights reserved)***

of the temperature do not show relevant differences over the radial direction, the axial velocity field is significantly affected by the presence of the blade leading edge in the SBES model. The corresponding contour plot highlights how the central portion of the cross section is affected by an important blockage effect due to the presence of the blade, compensated by an acceleration of the flow away from the leading edge. This different behavior also reflects into a steeper shape of the SBES radial profile from 15% to 70% of the span and a weaker hub-side blockage. Although the SBES conducted here may give a simplistic picture due to 1-to-1 burner-NGV ratio, it does reveal a physical phenomenon that may not have a relevant impact on the combustion chamber LES, but it may have one on how the aero-thermal field develops in the NGV.

Anyhow, as previously discussed, the application of 2D boundary condition maps in RANS is a step forward with respect to more simplified approaches usually adopted during the design phase where a simple 1D profile may be applied at the inlet and the blockage effect of Figure 2 is ignored.

The availability of a coupled SBES allows to extend the analysis of Figure 2 to quantities relevant to the turbulent flow characteristics. Here, the characteristic turbulent length scale, calculated according to Eq. 1, is considered as a key parameter, as it governs the turbulence decay:

$$l_t = C_\mu \frac{k^{3/2}}{\varepsilon} = \frac{\sqrt{k}}{\omega} \quad (1)$$

with $C_\mu = 0.09$. While in the RANS formulation the turbulent kinetic energy $k$ and the turbulent dissipation rate ε and turbulence frequency $\omega$ are directly available, in the SBES case they have to be derived from the solution. While the resolved turbulent kinetic energy is calculated leveraging the time-average values of the instantaneous velocity components, the sub-grid scale contribution is determined with the help of Eq. 2 that derives from the subgrid scale model:

$$k_{SGS} = \frac{\left(0.18\Delta^{\frac{1}{3}} \cdot S\right)^2}{0.3} \quad (2)$$

where Δ is the local cell volume and $S$ represents the local strain rate magnitude. The turbulent dissipation rate, acting exclusively at sub-grid scale in the LES-resolved part of the solution, is calculated as:

$$\varepsilon_{SGS} = \frac{\mu_{eff}}{\rho}\left(\frac{\partial u_i}{\partial x_j}\right)^2 \quad (3)$$

Figure 3 shows the turbulent length scale for both SBES and RANS on five planes (P39.5, P0, P1, P2, P3) orthogonal to the


Copyright © 2022 by ASME and Baker Hughes

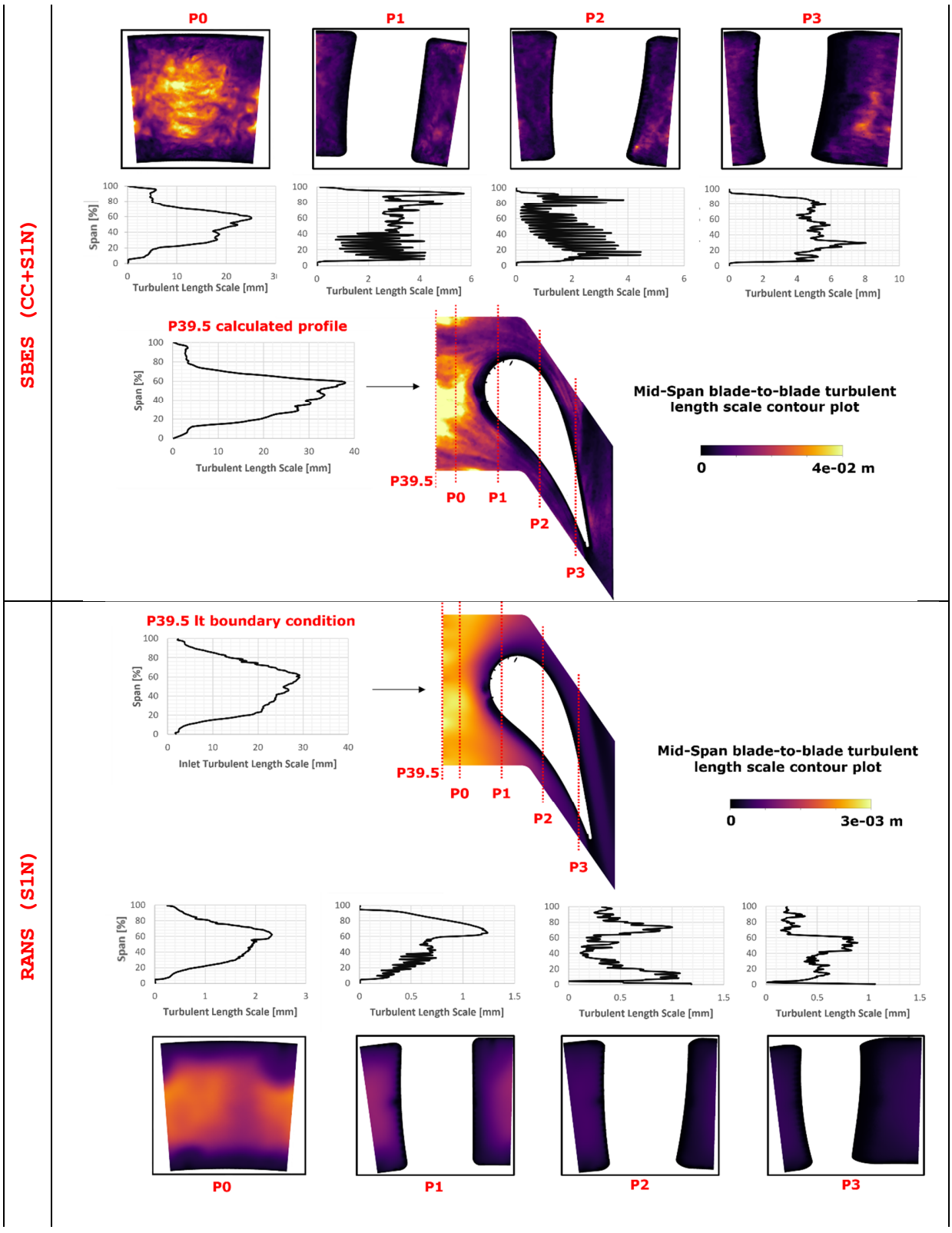


***Figure 3**. Analysis of the turbulent length scale on five planes (P39.5, P0, P1, P2, P3) orthogonal to the machine axis derived from the SBES (Top) and the RANS (Bottom) case. In the latter case, a sharp decreasing of $l_t$ is present right downstream the p39.5 location .* ***(© 2022 Baker Hughes Company – All rights reserved)***


Copyright © 2022 by ASME and Baker Hughes

machine axis, as well as the 1D profiles obtained by an azimuthal average of the 2D plots. The radial profile of the turbulent length scale at P39.5 from SBES is very similar to the one extracted from RANS. It is fairly instructive to observe that in the LES results, from which the inlet boundary conditions for the RANS have been derived, the maximum value of the turbulent length scale is close to 30 mm at 60% of the span. In the SBES model the peak is located at the same span but with a magnified amplitude. This is an additional proof that the set of boundary conditions employed for the RANS calculation is accurate.

More importantly, Figure 3 describes the evolution of the turbulent length scale inside the NGV for the two proposed approaches. Such quantity is displayed on a blade-to-blade surface located at 50% of the radial span and at four different cross sections downstream of the p39.5 plane. In particular, plane-0 (P0) is located in between the p39.5 and the leading edge of the blade, while P2 is positioned at the throat section.

The main finding of the analysis is that, despite the similarity of $l_t$ at plane p39.5 that enforces the inlet boundary condition, in RANS the turbulent length scale experiences a much steeper decay that is already visible at P0. Here, the turbulent length scale peak is reduced to approximately 2 mm, one order of magnitude smaller than the characteristic size at the inlet. Proceeding streamwise through the vane, the $l_t$ experiences a progressive reduction due to the flow expansion and the consequent strain of turbulent field. Conversely, the profiles predicted by the SBES approach show a significant decay of the turbulent length scale only inside the first stage nozzle due to the effect of the favorable pressure gradient, while $l_t$ shows a mild reduction before the leading edge where the pressure gradient kicks in. Inside the vane, the minimum of $l_t$ (~3mm) is reached at P2 location where the velocity of the flow reaches its maximum. To understand the reason for such difference, reports the circumferentially averaged radial profiles of the turbulent dissipation rate at plane P0. Focusing on the trends far from the walls, it is demonstrated that the turbulent dissipation rate predicted by the RANS largely overestimates the $\varepsilon_{SGS}$ from Eq. 3. Two equation models are known to suffer from excessive turbulence decay, especially when enforcing the integral length scale extracted from a LES. LES resolves the wide range of

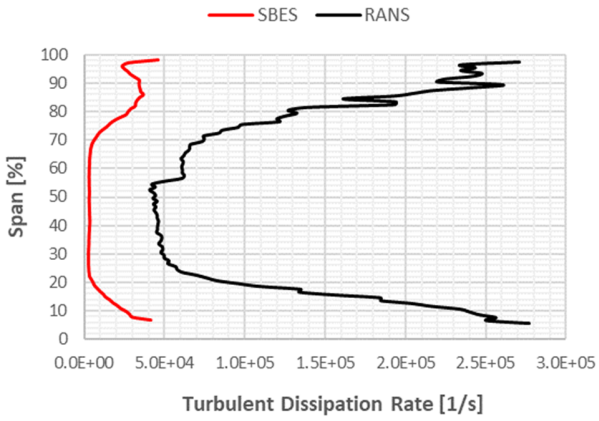


***Figure 4**. Turbulent dissipation rate along the span at P0 location: the RANS is affected by a higher dissipation, producing a fast decay of the turbulence and leading to a lower characteristic length scale.* ***(© 2022 Baker Hughes Company – All rights reserved)***

scales and does not associate any energy dissipation to the large values of $l_t$, but only to the smaller scales that are modelled separately. RANS is unable to discern the different contributions across a very wide range of $l_t$, and ultimately overestimates the decay of turbulence. Moreover, Figure 3 shows values of $l_t$ at P39.5 that are comparable with the NGV pitch at midspan, and a simple RANS model is definitely not suited to model the effect of macro-scale turbulence on the mean flow field. Relying on a pure LES solution in the core of the flow, the SBES model is surely more accurate than steady- state RANS solutions. This means that, when dealing with RANS, a strong under-estimation of the interaction between the main flow turbulent structures and the film cooling of the blade can be expected. Such kind of analysis will be carried out in the next paragraph.

Evaluation of the airfoil loads and adiabatic effectiveness

In order to better compare the two simulations, the airfoil loads in terms of isentropic Mach number at 25%, 50% and 75% of the span have been reported in Figure 5 for both the RANS and SBES calculations.

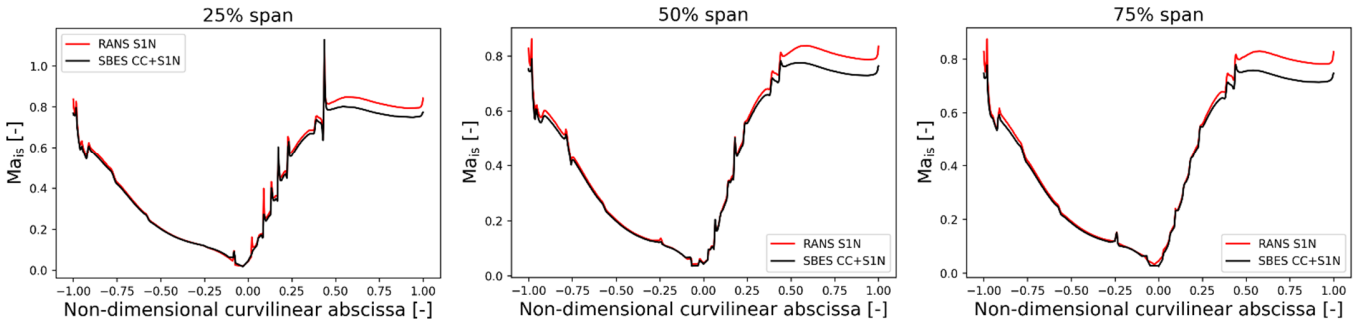


***Figure 5.** Isentropic Mach number on the NGV at 25%, 50%, 75% of the span. X=-1 corresponds to the trailing edge pressure side, X=0 is the leading edge, while X=1 is the trailing edge suction side.* ***(© 2022 Baker Hughes Company – All rights reserved)***


Copyright © 2022 by ASME and Baker Hughes

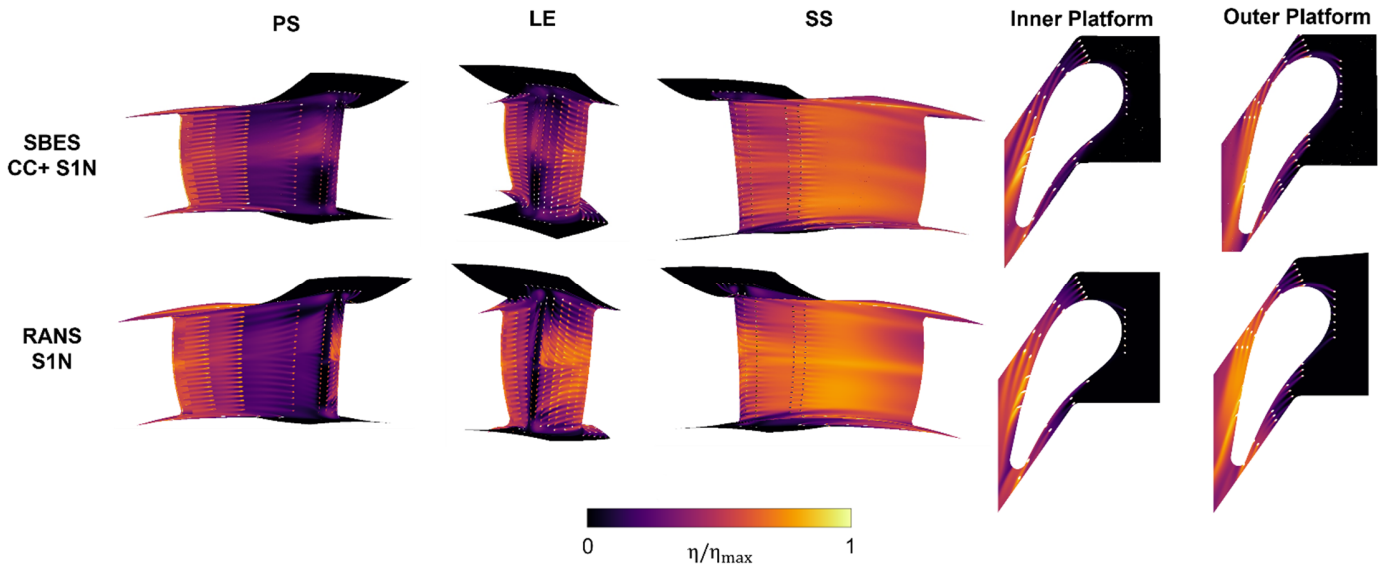


***Figure 6**. SBES-obtained time averaged adiabatic film-cooling effectiveness contours on the NGV and on the endwalls (Top) compared against RANS (Bottom). **(© 2022 Baker Hughes Company – All rights reserved)***

As can been seen, the two approaches SBES and RANS predict very similar. However, some differences emerge on the SS, especially on the second half of the vane after the throat. Moreover, these differences grow with span. This behavior might be attributed to the different loss mechanisms between SBES and RANS, especially in modeling the interaction between the main flow and the film cooling injections and in predicting separated flows as well. In fact, it is to be noted that such divergent behavior occurs downstream of the last film cooling row on the suction side surface of the airfoil and in correspondence of the throat section.

On the contrary, more consistent differences can be found by focusing on the prediction of the adiabatic film-cooling effectiveness. In Figure 6 the distribution of the non-dimensional adiabatic film cooling effectiveness on the vane is reported. As can be seen, the behavior of the film cooling is quite different between the two cases. Looking at the leading edge (LE) region, the RANS case predicts a very non-uniform effectiveness, especially on the LE, where a large part of the airfoil is left uncovered. On the other hand, in the SBES case, the presence of such areas seems to remain limited to the high and low values of span as can be noted especially by looking at the distribution of adiabatic effectiveness on the PS.

A further interesting difference is the position of the stagnation line, which is nearly straight in the RANS case, while it is highly distorted in the SBES solution. This is induced by the incoming swirled main flow, the impact of which is captured only by the scale resolving simulation. Relatively to the same aspect, also the coolant distribution on the PS surface looks influenced by the different representation of the main flow impact. In fact, while the RANS predicts a quite uniform coverage over the radial coordinate and all along the airfoil abscissa, the SBES simulation highlights a strongly non-uniform jets spreading. These look to be strongly conveyed towards the airfoil midspan, with reduced coolant traces at inner and outer radii.

Furthermore, the discrepancy in the distribution of film cooling between the two simulations is particularly evident by focusing on the region at 50% of the span on the SS surface. As a matter of fact, the RANS highlights an accumulation of film cooling for the entire length of the SS, a behavior that is not evident in the SBES case, which instead predicts a much more homogeneous coverage.

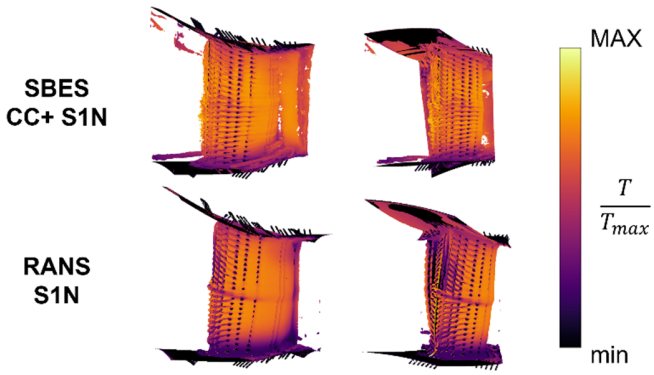


***Figure 7**. Q-criterion isosurfaces ($10^8$) colored by static temperature for the SBES-obtained time averaged solution (Top) and for the RANS (Bottom). **(© 2022 Baker Hughes Company – All rights reserved)***

In order to further highlight the presence of an accumulation of film cooling at 50% of the span for the RANS case, Figure 7 shows the Q-criterion [47] isosurfaces for both simulations,


Copyright © 2022 by ASME and Baker Hughes

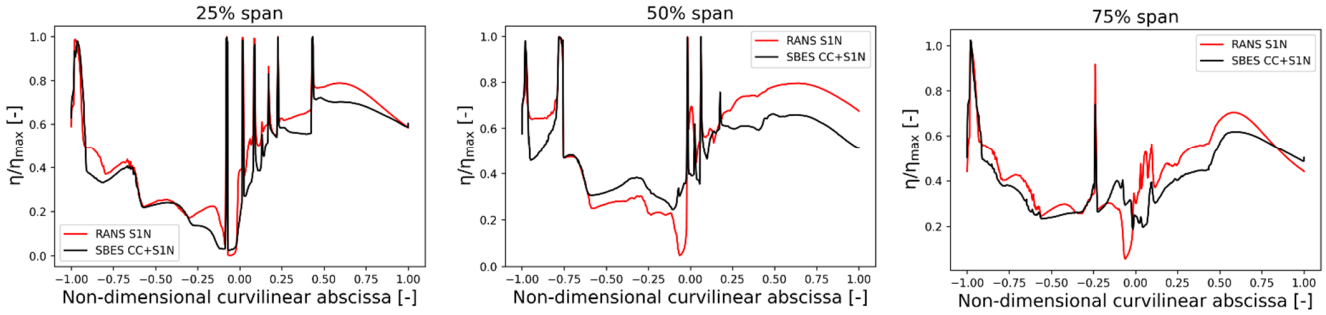


***Figure 8.*** *Adimensional adiabatic effectiveness on the NGV at 25%, 50%, 75% of the span. X=-1 corresponds to the trailing edge pressure side, X=0 is the leading edge, while X=1 is the trailing edge suction side.* ***(© 2022 Baker Hughes Company – All rights reserved)***

colored based on the temperature value. This discrepancy that emerged between the two simulations can be attributed to the different modeling between SBES and RANS as the latter tends to under-predict turbulent mixing and so to amplify the presence of these flow structures, which are generated as a consequence of the manufacturing process applied to the film cooling holes. In fact, it is to be noted that the axis of the showerhead holes placed in the higher span half is partly inward inclined, while the opposite applies to those in the lower span half.

To go into more details, the profiles of adiabatic effectiveness over the airfoil plotted as function of the non-dimensional curvilinear abscissa for both cases have been also reported in Figure 8. As matter of fact, at 50% of the span, it can be clearly noted how RANS deviates from the prediction of the SBES, underestimating the adiabatic effectiveness at the LE and PS and overestimating it on the SS, as previously described. However, this behavior is not observed for different span values: in fact, at 25 and 75% of the span, it can be noted that the RANS generally tends to assume values of adiabatic effectiveness that are higher than those of SBES, especially on the SS. This demonstrates that, as expected and already demonstrated in the literature [34,35], it is essential to include the effects of unsteadiness on turbulent mixing, which otherwise would be strongly under-predicted.

A similar reasoning can be also applied to the endwalls: as can be seen from Figure 6, RANS seems to overestimate the adiabatic effectiveness especially on the region adjacent to the SS, where the contours show more homogeneous and globally higher values even far from the vane surface.

Another interesting aspect to consider in the integrated combustor-NGV calculation regards the presence of the cooling flow coming from the nuggets. In fact, if in the case of the NGV stand-alone case, this aspect is simply treated as a temperature distortion at the inlet plane, in the case of the integrated combustor-NGV simulation it is instead possible to differentiate this flow from the main one, thus being able to more easily evaluate its impact on the first stator. In this regard, Figure 9 shows the dimensionless adiabatic effectiveness due to the cooling flows coming from the nuggets for the SBES case and RANS case as well. As expected, in both cases, the presence of these flows has a beneficial impact on the endwalls but their effect on the nozzle remains limited to the regions at low and

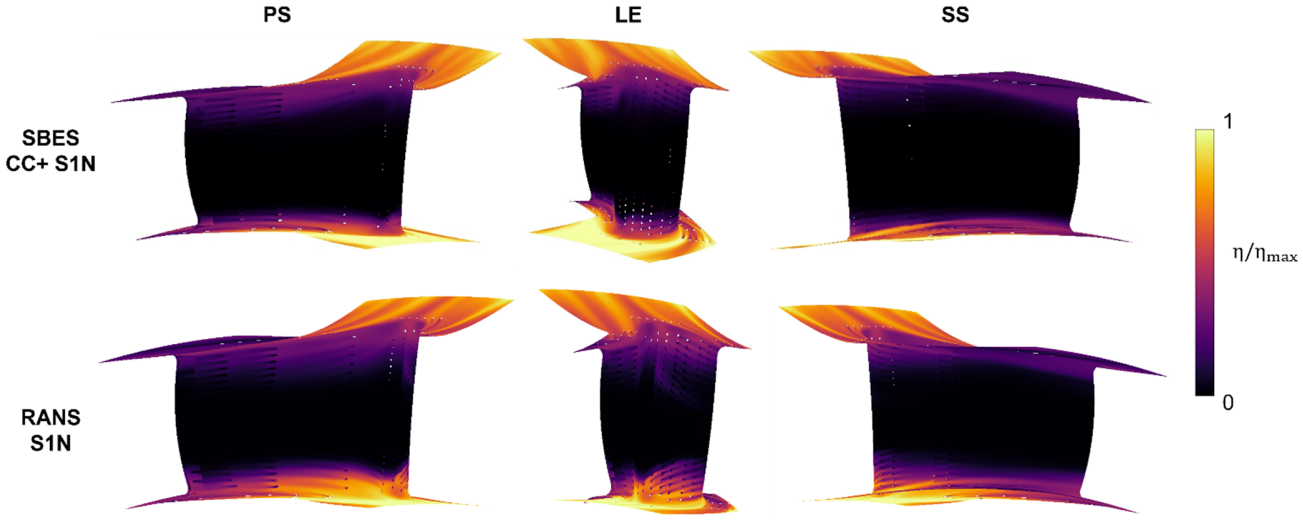


***Figure 9****. SBES-obtained time averaged adiabatic effectiveness contours on the NGV and on the endwalls referred to the cooling flow coming from the nuggets.* ***(© 2022 Baker Hughes Company – All rights reserved)***


Copyright © 2022 by ASME and Baker Hughes

high values of span. As a matter of fact, their interaction with the central part of the NGV is mostly negligible, especially near the inner wall. However, the slightly greater interaction of the flow with the NGV near the outer wall region that can be observed in both cases can be mainly attributed to a greater curvature of the wall. In particular, in the RANS case it can be seen how the cooling flow tends to extend more towards the center of the vane than in the SBES simulation, especially near the inner wall region, where there is a greater coverage of the coolant, especially on the LE. This behavior can be attributed to the strong underprediction of turbulent mixing in the case of RANS which, as already noted in Fig. 6, has an impact on the interaction between the main flow and the film cooling.

## CONCLUSIONS

This paper reports the numerical investigation, performed on a realistic annular geometry with operating conditions, of the interaction between the combustion chamber and the turbine nozzle. The cooling system of the NGV has also been included in order to study the interaction between the film cooling jets and the main flow coming from the combustor. To do so, the numerical simulation of a fully integrated combustor-NGV, performed by using a SBES, is compared with an isolated NGV simulation, carried out by using a RANS approach.

First, the different conditions existing on the 39.5 plane, that represents the interface plane between the combustor and the NGV, were investigated. It has been noted that, although there are no large differences in terms of temperature distribution, more evident differences can be observed in the axial velocity: In fact, because of the blocking effect of the stator leading edge the velocity distribution is altered in the SBES case with respect to the RANS one, the inlet boundary conditions of which has been extracted from a precursor LES of the stand-alone combustor without S1N.

Moreover, despite the initial similarity in terms of turbulent length scale between the two simulations at plane 39.5, it has been observed that $l_t$ in RANS case experiences a much steeper decay, as demonstrated by analyzing four different cross sections downstream the p39.5 plane. This can be attributed to the higher turbulent dissipation rate of the RANS calculation that can be already observed even before reaching the LE (plane p0), thus producing a fast decay of the turbulence. This strong underprediction of the turbulent mixing has also an impact on the interaction between the main flow and the film cooling. As a matter of fact, it has been demonstrated that, not only the RANS simulation generally tends to overestimate the adiabatic effectiveness along the vane, but, compared to the SBES, it also provides a different distribution of the film cooling traces between PS and SS: this leads to a less homogenous coverage, leaving areas of the vane locally unprotected, as can be seen on LE and PS, while overpredicting the effectiveness in others, especially on the SS, where an accumulation of film cooling is evident at the 50% of the span. Moreover, studying the impact that the cooling flow from the nuggets have on the vane, it is noted that both for the SBES and for the RANS cases they interact only with regions near the endwalls which means a very limited portion of the NGV span. However, also in this case, the RANS overestimates the interaction of the film cooling with the vane, due to the strong underprediction of the turbulent mixing, providing a greater coverage of the film cooling especially on the LE. In conclusion, the analyses the coupled and decoupled simulation reveal that, the behavior of the film cooling differs considerably between the two cases, indicating that an integrated approach based on high-fidelity turbulence is highly recommendable for the accurate prediction of the adiabatic effectiveness.

## REFERENCES


[1] Cha, C. M., Hong, S., Ireland, P. T., Denman, P., and Savarianandam, V., 2012, "Experimental and Numerical Investigation of Combustor-Turbine Interaction Using an Isothermal, Nonreacting Tracer," J. Eng. Gas Turbines Power, **134**(8).

[2] Cha, C. M., Ireland, P. T., Denman, P. A., and Savarianandam, V., 2012, "Turbulence Levels Are High at the Combustor-Turbine Interface," *Turbo Expo: Power for Land, Sea, and Air*, pp. 1371–1390.

[3] Krichbaum, A., Schiffer, H.-P., and Werschnik, H., 2015, "The Influence of Combustor Swirl on Turbine Stator Endwall Heat Transfer and Film Cooling Effectiveness in a 1.5-Stage Axial Turbine," ISABE 2015 (Awatef Hamed, Fac. Work Res. Coll. Eng. Appl. Sci.

[4] Salvadori, S., Ottanelli, L., Jonsson, M., Ott, P., and Martelli, F., 2012, "Investigation of High-Pressure Turbine Endwall Film-Cooling Performance under Realistic Inlet Conditions," J. Propuls. Power, **28**(4), pp. 799–810.

[5] Giller, L., and Schiffer, H.-P., 2012, "Interactions between the Combustor Swirl and the High Pressure Stator of a Turbine," *Turbo Expo: Power for Land, Sea, and Air*, pp. 1401–1415.

[6] Pyliouras, S., Schiffer, H.-P., Janke, E., and Willer, L., 2012, "Effects of Non-Uniform Combustor Exit Flow on Turbine Aerodynamics," *Turbo Expo: Power for Land, Sea, and Air*, pp. 1691–1701.

[7] Schmid, G., Krichbaum, A., Werschnik, H., and Schiffer, H.-P., 2014, "The Impact of Realistic Inlet Swirl in a 1 1/2 Stage Axial Turbine," *Turbo Expo: Power for Land, Sea, and Air*, p. V02CT38A045.

[8] Zhang, X., and Chen, F., 2020, "Influence of Non-Uniform Inflow Swirl and Hot Streak on Turbine Vane," Aerosp. Syst., **3**(2), pp. 79–85.

[9] Mansuori, Z., and Belamadi, R., 2021, "The Influence of Inlet Swirl Intensity and Hot-Streak on Aerodynamics and Thermal Characteristics of a High Pressure Turbine Vane," Chinese J. Aeronaut.

[10] Wang, Z., Wang, D., Wang, Z., and Feng, Z., 2018, "Heat Transfer Analyses of Film-Cooled HP Turbine Vane Considering Effects of Swirl and Hot Streak," Appl.



Copyright © 2022 by ASME and Baker Hughes

Therm. Eng., **142**, pp. 815–829.

[11] Qureshi, I., Smith, A. D., and Povey, T., 2013, "Hp Vane Aerodynamics and Heat Transfer in the Presence of Aggressive Inlet Swirl," J. Turbomach., **135**(2), p. 21040.

[12] Werschnik, H., Hilgert, J., Wilhelm, M., Bruschewski, M., and Schiffer, H.-P., 2017, "Influence of Combustor Swirl on Endwall Heat Transfer and Film Cooling Effectiveness at the Large Scale Turbine Rig," J. Turbomach., **139**(8).

[13] Insinna, M., Griffini, D., Salvadori, S., and Martelli, F., 2014, "Conjugate Heat Transfer Analysis of a Film Cooled High-Pressure Turbine Vane under Realistic Combustor Exit Flow Conditions," *Turbo Expo: Power for Land, Sea, and Air*, p. V05AT11A007.

[14] Griffini, D., Insinna, M., Salvadori, S., and Martelli, F., 2016, "Clocking Effects of Inlet Nonuniformities in a Fully Cooled High-Pressure Vane: A Conjugate Heat Transfer Analysis," J. Turbomach., **138**(2), p. 21006.

[15] Khanal, B., He, L., Northall, J., and Adami, P., 2013, "Analysis of Radial Migration of Hot-Streak in Swirling Flow through High-Pressure Turbine Stage," J. Turbomach., **135**(4), p. 41005.

[16] Wissink, J. G., Michelassi, V., and Rodi, W., 2004, "Heat Transfer in a Laminar Separation Bubble Affected by Oscillating External Flow," Int. J. heat fluid flow, **25**(5), pp. 729–740.

[17] Roux, S., Cazalens, M., and Poinsot, T., 2008, "Outlet-Boundary-Condition Influence for Large Eddy Simulation of Combustion Instabilities in Gas Turbines," J. Propuls. Power, **24**(3), pp. 541–546.

[18] Klapdor, E. V., 2011, "Simulation of Combustor-Turbine Interaction in a Jet Engine."

[19] Morata, E. C., 2012, "Impact of the Unsteady Aerothermal Environment on the Turbine Blades Temperature," Institut National Polytechnique de Toulouse-INPT.

[20] Boudier, G., Gicquel, L. Y. M., Poinsot, T., Bissieres, D., and Bérat, C., 2007, "Comparison of LES, RANS and Experiments in an Aeronautical Gas Turbine Combustion Chamber," Proc. Combust. Inst., **31**(2), pp. 3075–3082.

[21] James, S., Zhu, J., and Anand, M. S., 2006, "Large-Eddy Simulations as a Design Tool for Gas Turbine Combustion Systems," AIAA J., **44**(4), pp. 674–686.

[22] Pope, S. B., 2004, "Ten Questions Concerning the Large-Eddy Simulation of Turbulent Flows," New J. Phys., **6**(1), p. 35.

[23] Koupper, C., Bonneau, G., Gicquel, L., and Duchaine, F., 2016, "Large Eddy Simulations of the Combustor Turbine Interface: Study of the Potential and Clocking Effects," *Turbo Expo: Power for Land, Sea, and Air*, p. V05BT17A003.

[24] Thomas, M., Duchaine, F., Gicquel, L., and Koupper, C., 2017, "Advanced Statistical Analysis Estimating the Heat Load Issued by Hot Streaks and Turbulence on a High-Pressure Vane in the Context of Adiabatic Large Eddy Simulations," *Turbo Expo: Power for Land, Sea, and Air*, p. V02BT41A041.

[25] Thomas, M., Dombard, J., Duchaine, F., Gicquel, L., and Koupper, C., 2019, "Large Eddy Simulation of Combustor and Complete Single-Stage High-Pressure Turbine of the FACTOR Test Rig," *Turbo Expo: Power for Land, Sea, and Air*, p. V02AT45A016.

[26] Gicquel, L. Y. M., Staffelbach, G., and Poinsot, T., 2012, "Large Eddy Simulations of Gaseous Flames in Gas Turbine Combustion Chambers," Prog. energy Combust. Sci., **38**(6), pp. 782–817.

[27] Menter, F., and Egorov, Y., 2005, "A Scale Adaptive Simulation Model Using Two-Equation Models," *43rd AIAA Aerospace Sciences Meeting and Exhibit*, p. 1095.

[28] Menter, F. R., and Egorov, Y., 2006, "Revisiting the Turbulent Scale Equation," *IUTAM Symposium on One Hundred Years of Boundary Layer Research*, pp. 279–290.

[29] Spalart, P. R., 1997, "Comments on the Feasibility of LES for Wings, and on a Hybrid RANS/LES Approach," *Proceedings of First AFOSR International Conference on DNS/LES*.

[30] Bacci, T., Lenzi, T., Picchi, A., Mazzei, L., and Facchini, B., 2018, "Flow Field and Hot Streak Migration through High Pressure Cooled Vanes with Representative Lean Burn Combustor Outflow," *Turbo Expo: Power for Land, Sea, and Air*, p. V05CT17A009.

[31] Bacci, T., Becchi, R., Picchi, A., and Facchini, B., 2019, "Adiabatic Effectiveness on High-Pressure Turbine Nozzle Guide Vanes under Realistic Swirling Conditions," J. Turbomach., **141**(1), p. 11009.

[32] Andreini, A., Bacci, T., Insinna, M., Mazzei, L., and Salvadori, S., 2017, "Hybrid RANS-LES Modeling of the Aerothermal Field in an Annular Hot Streak Generator for the Study of Combustor--Turbine Interaction," J. Eng. Gas Turbines Power, **139**(2).

[33] Miki, K., Moder, J., and Liou, M.-S., 2018, "Computational Study of Combustor--Turbine Interactions," J. Propuls. Power, **34**(6), pp. 1529–1541.

[34] Cubeda, S., Mazzei, L., Bacci, T., and Andreini, A., 2018, "Impact of Predicted Combustor Outlet Conditions on the Aerothermal Performance of Film-Cooled HPT Vanes," *Turbo Expo: Power for Land, Sea, and Air*, p. V05CT17A005.

[35] Cubeda, S., Mazzei, L., and Andreini, A., 2019, "External Heat Transfer on Nozzle Guide Vanes under Highly Swirled Combustor Outlet Flow," *13 Th European Conference on Turbomachinery Fluid Dynamics \& Thermodynamics*.

[36] Verma, I., Rida, S., Zori, L., Basani, J., Kamrath, B., and Brandt, D., 2021, "Modeling of Combustor-Turbine Vane Interaction Using Stress-Blended Eddy Simulation," *Turbo Expo: Power for Land, Sea, and Air*, p. V02DT39A008.

[37] Menter, F., 2016, "Stress-Blended Eddy Simulation

 Copyright © 2022 by ASME and Baker Hughes

(SBES)—A New Paradigm in Hybrid RANS-LES Modeling," *Symposium on Hybrid RANS-LES Methods*, pp. 27–37.

[38] Nassini, P. C., Pampaloni, D., Meloni, R., and Andreini, A., 2021, "Lean Blow-out Prediction in an Industrial Gas Turbine Combustor through a LES-Based CFD Analysis," Combust. Flame, **229**, p. 111391.

[39] Nassini, P. C., Pampaloni, D., Andreini, A., and Meloni, R., 2019, "Large Eddy Simulation of Lean Blow-Off in a Premixed Swirl Stabilized Flame," *Turbo Expo: Power for Land, Sea, and Air*, p. V04AT04A053.

[40] Romano, S., Meloni, R., Riccio, G., Nassini, P. C., and Andreini, A., 2021, "Modeling of Natural Gas Composition Effect on Low NOx Burners Operation in Heavy Duty Gas Turbine," J. Eng. Gas Turbines Power, **143**(3), p. 31018.

[41] Meloni, R., Gori, S., Andreini, A., and Nassini, P. C., 2021, "CO Emission Modeling in a Heavy Duty Annular Combustor Operating With Natural Gas," J. Eng. Gas Turbines Power, **144**(1), p. 11011.

[42] Meloni, R., Andreini, A., and Nassini, P. C., 2021, "A Novel Large-Eddy Simulation-Based Process for NOx Emission Assessment in a Premixed Swirl Stabilized Combustion System," J. Eng. Gas Turbines Power, **144**(1), p. 11010.

[43] Tay-Wo-Chong, L., Scarpato, A., and Polifke, W., 2017, "LES Combustion Model with Stretch and Heat Loss Effects for Prediction of Premix Flame Characteristics and Dynamics," *Turbo Expo: Power for Land, Sea, and Air*, p. V04AT04A029.

[44] Smith, G. P., Golden, D. M., Frenklach, M., Moriarty, N. W., Eiteneer, B., Goldenberg, M., Bowman, C. T., Hanson, R. K., Song, S., Gardiner Jr, W. C., and others, 1999, "GRI 3.0 Mechanism," Gas Res. Inst. (http//www. me. berkeley. edu/gri_mech).

[45] Meloni, R., Ceccherini, G., Michelassi, V., and Riccio, G., 2019, "Analysis of the Self-Excited Dynamics of a Heavy-Duty Annular Combustion Chamber by Large-Eddy Simulation," J. Eng. Gas Turbines Power, **141**(11), p. 111016.

[46] Cerutti, M., Giannini, N., Ceccherini, G., Meloni, R., Matoni, E., Romano, C., and Riccio, G., 2018, "Dry Low NOx Emissions Operability Enhancement of a Heavy-Duty Gas Turbine by Means of Fuel Burner Design Development and Testing," *Turbo Expo: Power for Land, Sea, and Air*, p. V04BT04A029.

[47] Jeong, J., and Hussain, F., 1995, "On the Identification of a Vortex," J. Fluid Mech., **285**, pp. 69–94.

 Copyright © 2022 by ASME and Baker Hughes